VI International Conference on Computational Methods in Marine Engineering
MARINE 2015
F. Salvatore, R. Broglia and R. Muscari (Eds)

A GENERALISED FULLY UNSTEADY HYBRID RANS/BEM MODEL FOR MARINE PROPELLER FLOW SIMULATIONS

F. SALVATORE*, D. CALCAGNI†, R. MUSCARI†, R. BROGLIA†

*Maritime Technology Research Institute
National Research Council (CNR-INSEAN)
Via di Vallerano, 139, 00128 Rome, Italy
e-mail: francesco.salvatore@cnr.it, web page: http://www.insean.cnr.it

Key words: Marine propulsion, hydrodynamics, Hybrid RANSE/BEM

Abstract. A generalised hybrid RANSE/BEM model for the analysis of hull/propeller interaction in ship hydrodynamics problems at reduced computational cost is presented. Akin to standard hybrid RANSE/BEM models, the coupling between viscous and inviscid-flow solvers is based on a volume-force/effective-inflow approach. The generalization consists in coupling a time-accurate solution by BEM of the unsteady flow around the rotating propeller with the solution of the surrounding viscous-flow by unsteady RANSE to account for transient-flow propeller perturbation. The methodology is validated through numerical applications to a simple case study describing a propeller in uniform flow conditions. Numerical results by the proposed hybrid RANSE/BEM model are compared with results by full-RANSE simulations and the capability of the methodology to correctly describe transient propeller flow perturbation to a surrounding viscous flow is investigated.

1 INTRODUCTION

The interest for energy efficient solutions in marine transport motivates the necessity to improve hydrodynamics modelling tools for the analysis of non-conventional propulsion systems and to correctly describe the interaction between propulsors and innovative hull-forms over a wide range of operating conditions. Computational Fluid Dynamics (CFD) tools based on the numerical solution of the Navier-Stokes equations have proved the capability to correctly simulate screw-propeller operation in the turbulent hull wake flow but simulation effort is an issue. Reliable results are obtained at huge computational costs in terms of both computational resources and human effort to build quality grids around the hullform and propeller blades. As a consequence, propelled ship flow simulations by Reynolds Averaged Navier-Stokes Equations (RANSE) and other CFD models are generally feasible only for analysis and verification whereas overall computational costs are unaffordable for design and optimization studies.

An approach to reduce the computational effort is to replace actual propeller modelling by the viscous-flow solver with an actuator disk model capable to approximately account for propeller effects by source terms in the momentum equations that simulate screw suction and swirl. Since early formulations ([1], [2]) where basic models where used to predict propeller induction, the methodology has been refined and viscous-flow solvers (typically, RANSE) have been interfaced with inviscid-flow propeller models by lifting-line, vortex-lattice methods ([3]). Recently, actuator disk models based on Boundary Element Methods (BEM) have become popular and the methodology is often referred to as hybrid RANSE/BEM model. Reliable estimates of global propulsion factors (propeller rps, power) are obtained, whereas propeller loading is averaged in time and local details of transient flow perturbation induced by the propeller are missed. Examples of applications are given in [4] and in [5] where the BEM solver used is the same as in the present work.

Aim of the present paper is to describe a computational methodology to generalize the hybrid RANSE/BEM model concept. Akin to standard hybrid RANSE/BEM models, the coupling between viscous and inviscid-flow solvers is based on a volume-force/effective-inflow approach. The generalization consists in coupling a time-accurate solution by BEM of the unsteady flow around the rotating propeller with the solution of the surrounding viscous-flow by a RANSE that is run in unsteady mode to fully account for transient-flow propeller perturbation. Propeller blades are not described as solid boundaries in the computational domain where RANS equations are solved. Hydrodynamic forces on propeller blade surface are determined by BEM and recast as volume forces distributed on the actual position occupied by blades during rotation. Volume forces are plugged as source terms in the momentum equation that is solved by unsteady RANSE. The velocity distribution by RANSE is used to determine the total inflow to the propeller. At each time step, the inflow to the propeller is evaluated as difference between the velocity distribution by RANSE and time-accurate propeller induced velocity by BEM. The resulting distribution (*effective inflow*) is used to evaluate boundary conditions for BEM. The procedure is iterated to convergence. The present methodology differs from an existing hybrid RANSE/BEM model for unsteady flows proposed in [6] for the technique used to convert blade surface loading into volume forces and for the coupling strategy between viscous and inviscid flow solvers.

In the paper, the methodology is described with emphasis on the coupling strategy valid for transient flows. Next, results of the numerical application to the case of a propeller in open water conditions are presented. Comparing results by the hybrid RANSE/BEM model and those by full RANSE, the capability of the methodology to capture transient propeller flow perturbation to a surrounding viscous flow is clarified.

2 THEORETICAL MODEL

The proposed methodology is based on the assumption that the velocity field around a propeller can be decomposed into the perturbation induced by the propeller, $\mathbf{v}_P$ studied under inviscid, irrotational flow assumptions, and the surrounding viscous, rotational flow

$\mathbf{v}_R$. The irrotational velocity condition yields that $\mathbf{v}_P$ can be expressed through a scalar potential φ and hence the total velocity field reads $\mathbf{v} = \nabla\varphi + \mathbf{v}_R$.

2.1 Inviscid flow model by BEM

The inviscid-flow contribution describing propeller perturbation is studied by a boundary element model (BEM) for three-dimensional lifting bodies in arbitrary motion. A general formulation valid for potential/rotational velocity decompositions is given in [7], whereas here contributions from the rotational flow component to the velocity potential are neglected. The methodology is implemented into the PRO-INS solver for the analysis of conventional propellers in non-cavitating flows and cavitating flows, [8], [9], [11], and complex propulsors as ducted propellers, [10], podded and contra-rotating propellers [12].

Under potential flow assumptions, mass and momentum equations reduce, respectively, to the Laplace equation for the velocity potential, $\nabla^2\varphi = 0$, and the Bernoulli equation

$$\frac{\partial\varphi}{\partial t} + \frac{1}{2}\|\nabla\varphi + \mathbf{v}_I\| + \frac{p}{\rho} + gz_0 = \frac{1}{2}v_I^2 + \frac{p_0}{\rho}, \tag{1}$$

where p_0 is the free-stream reference pressure, $\mathbf{v}_I$ is the inflow to the propeller as observed from a frame of reference fixed with the propeller blades, and gz_0 is the hydrostatic head.

Following classical potential field theory, the Laplace equation for φ can be solved by a boundary integral representation (see, *e.g.*, [13])

$$E(\mathbf{x})\,\varphi(\mathbf{x}) = \oint_{\mathcal{S}_B}\left(\frac{\partial\varphi}{\partial n}G - \varphi\frac{\partial G}{\partial n}\right)d\mathcal{S} - \int_{\mathcal{S}_W}\Delta\varphi\frac{\partial G}{\partial n}d\mathcal{S} \tag{2}$$

where $\mathcal{S}_B$ denotes the propeller solid surface, $\mathcal{S}_W$ is the trailing wake and $\mathbf{n}$ is the unit normal to these surfaces. The symbol Δ denotes discontinuity of φ across the wake surface, and $G, \partial G/\partial n$ are unit source and dipoles in the unbounded three-dimensional space. Finally, $E(\mathbf{x})$ is a field function defined throughout the fluid domain and characterizing the case where $\mathbf{x}$ is inside the flow field ($E = 1$), on the solid boundary surface ($E = 1/2$) or inside the solid body ($E = 0$).

Boundary conditions for φ on the solid surface $\mathcal{S}_B$ are obtained by imposing impermeability, $\mathbf{v}\cdot\mathbf{n} = \mathbf{v}_B\cdot\mathbf{n}$, or ($\mathbf{v}_B$ being the velocity of body points from an inertial observer)

$$\frac{\partial\varphi}{\partial n} + \mathbf{v}_R\cdot\mathbf{n} = \mathbf{v}_B\cdot\mathbf{n} \tag{3}$$

In addition to this, a Kutta-type condition is enforced to impose convection along the wake surface $\mathcal{S}_W$ of the potential discontinuity between suction and pressure sides at blade trailing edge.

Combining the condition $\mathbf{v} = \nabla\varphi$, and Eqs. (1) to (3) yields that propeller induced velocity and pressure fields may be evaluated through a linear problem in which unknowns are located on boundary surfaces $\mathcal{S}_B$ and $\mathcal{S}_W$. Numerical solutions are obtained at reduced computational effort and negligible grid generation complexity.

Once φ on $\mathcal{S}_{_B}$ is known from the numerical solution of Eq. (2) and the pressure p is determined from Eq. (1), hydrodynamic forces acting on the propeller blades follow as

$$\mathbf{f} = \sum_{n=1}^{Z} \int_{\mathcal{S}_{B_n}} (-p\mathbf{n} + \tau\mathbf{t})\, d\mathcal{S}, \tag{4}$$

where $\mathcal{S}_{_{B_n}}$ $(n = 1, ...Z)$ denotes the surface of the n-th blade of a Z–bladed screw. Using a common approach in inviscid-flow models, the distribution of viscosity–induced tangential stress τ is estimated by using expressions that are valid for flat plates in laminar and turbulent flow at Reynolds number determined from propeller operating conditions.

Dealing with hybrid RANSE/BEM models, quantity $(-p\mathbf{n} + \tau\mathbf{t})$ in Eq. (4) denotes a force density on propeller blades that is recast as volume force distribution for inclusion as source term into the momentum equations of the RANSE model.

2.2 Viscous flow model by RANSE

The viscous flow surrounding the propeller is evaluated through the integration of the Unsteady Reynolds Averaged Navier–Stokes Equations (URANSE) in incompressible flow

$$\begin{aligned} &\nabla \cdot \mathbf{v} = 0 \\ &\frac{\partial \mathbf{v}}{\partial t} + (\mathbf{v} \cdot \nabla)\mathbf{v} = -\frac{1}{\rho}\nabla p + \nu\nabla^2\mathbf{v} + \mathbf{Q} \end{aligned} \tag{5}$$

where quantity $\mathbf{Q}$ denotes a source term describing propeller induced volume forces predicted by BEM. With the inclusion of propeller induction, equations (5) provide the total flow velocity $\mathbf{v}$. The numerical algorithm to solve Eq. (5) is implemented into the χ–$Navis$ code developed by CNR-INSEAN. The numerical model is based on a finite volume technique with pressure and velocity co–located at cell center. Viscous terms are integrated by a standard second order centered scheme, whereas for the convective and pressure terms a third order upwind scheme is chosen. Because of the treatment of the viscous terms, the scheme remains formally second order in space. The physical time–derivative in the governing equations is approximated by a second order accurate, three–point backward finite difference formula [14]. Turbulent viscosity is calculated by means of the one–equation model by Spalart & Allmaras.

No-slip boundary conditions are enforced at solid walls. At the inlet boundary the velocity is set to the undisturbed flow value, whereas at the outflow the pressure is set equal to zero.

The mesh built to discretize the fluid domain is composed by structured, partially overlapping blocks, and a chimera algorithm is used. In the present approach, the interpolation of the solution among different chimera subgrids is enforced in a *body-force* fashion. Specifically, at chimera cells a source term is added to the standard equations

$$\mathbf{q}^{n+1}_{\mathsf{chimera}} = \mathbf{q}^{n}_{\mathsf{chimera}} - \Delta t \left[\mathcal{R}^n + \frac{\kappa}{\delta}\left(\mathbf{q}^{n}_{\mathsf{chimera}} - \mathbf{q}^{n}_{\mathsf{interp}}\right)\right] \tag{6}$$

where $\mathbf{q}$ is the RANSE unknown vector, $\mathcal{R}$ is the vector of the residuals, $\kappa = \mathcal{O}(10)$ is a parameter chosen through numerical tests, and δ is the cell diameter [15, 16, 17].

The introduction of propeller effects via RANSE/BEM coupling is obatined by a formally equivalent approach as Eq. (6). Specifically, propeller blades are not represented as solid boundaries of the computational domain and a cylindrical grid block (*volume force block*) is placed to fill the propeller region. Volume forces $\mathbf{Q}$ describing propeller induction are distributed over this grid block and source term are added to the righ-hand side of the momentum equations to obtain

$$\mathbf{q}^{n+1}_{\mathsf{propeller}} = \mathbf{q}^{n}_{\mathsf{propeller}} - \Delta t \left[\mathcal{R}^n + \mathcal{Q}^n\right] \tag{7}$$

where $\mathcal{Q}^n$ denotes the volume force vector.

2.3 RANSE/BEM coupling

The coupling between viscous and inviscid-flow solutions is established through two main quantities exchanged by RANSE and BEM solvers:

- volume-forces $\mathbf{Q}$: recast hydrodynamic forces on propeller blade surface as source terms suitable for inclusion into a RANSE where blades are not explicitly solved;
- effective-inflow $\mathbf{v}_{R}$: the rotational inflow to the propeller necessary to correctly evaluate boundary conditions for BEM using Eq. (3).

The numerical procedure to determine volume forces from blade surface loading is described first. Consider a Cartesian coordinate system $(Ox_{F}y_{F}z_{F})$ fixed to an inertial frame with x axis parallel to propeller axis, as shown in Fig. 1. Denote by $\bar{S}_{B_k}$ $(k = 1, ..Z)$ the k–th blade mean surface determined by collapsing blade suction and pressure sides onto a single surface. At each time step, the position of an arbitrary point on $\bar{S}_{B_k}$ is uniquely determined through its axial position x_{F} and its projection on a plane $Oy_{F}z_{F}$ normal to propeller axis: the propeller disc plane is typically chosen. Polar coordinates r and θ are used on this plane, see left Fig. 1.

Equation (4) may be rewritten as

$$\mathbf{f} = \sum_{k=1}^{Z} \int_{\bar{S}_{B_k}} -\mathbf{q}_k \, d\mathcal{S}, \qquad \text{with} \quad \mathbf{q}_k = (p\mathbf{n} - \tau\mathbf{t})^{suct}_{k} + (p\mathbf{n} - \tau\mathbf{t})^{press}_{k}. \tag{8}$$

Vector quantities $\mathbf{q}_k$ represent surface distributions of propeller loading acting on blade mean surfaces (dimensions are force per unit surface). Distributions are uniquely associated through coordinates x_{F}, r, θ to the actual position of blades. The minus sign in Eq. (8) is put to stress that quantity $\mathbf{q}_k$ denotes the hydrodynamic force that the solid body (the propeller) acts on the fluid, whereas $\mathbf{f}$ is the force that the fluid acts onto the solid body.

A time-accurate representation of $\mathbf{q}_k$ as a volume–force distribution is easily obtained. At each time step, quantity $\mathbf{q}_k = \mathbf{q}_k(x_F, r, \theta, t)$ is interpolated along r, θ at centroids of cells of the volume force block of the RANSE grid. This block is cylindrical with axis parallel to the x_F axis, right Fig. 1. Volume force value $\hat{\mathbf{q}}_{l,m,n}$ interpolated at an arbitrary grid cell $H_{l,m,n}$ is then distributed in axial direction over a suitable number of grid cells over a layer of axial extension $2\Delta n$ by imposing a local load conservation condition

$$\sum_n \hat{\mathbf{q}}'_{l_0,m_0,n}\, \xi_{l_0,m_0,n}\, \Delta x_{l_0,m_0,n} \;=\; \hat{\mathbf{q}}_{l_0,m_0,n_0} \qquad n_0 - \Delta n < n < n_0 + \Delta n, \tag{9}$$

where $\Delta x_{l,m,n}$ denotes the axial extension of cell (l, m, n) and $\xi_{l,m,n}$ is a weight function. In the present work, $\xi_{l,m,n}$ is determined by assuming a Gaussian distribution along the axial direction x_F. The width of the Gaussian curve is kept small to ensure that volume forces are distributed over an axial layer whose length is comparable with the thickness of the solid blade along the same direction. In the present work, a width of $0.075D$ is chosen since smaller values tend to reduce the convergence rate of RANSE. The interpolation technique is very fast and determines volume force distributions that reflect at each time step the actual position and local intensity of blade loading over the propeller disk, as shown in results described in the next section.

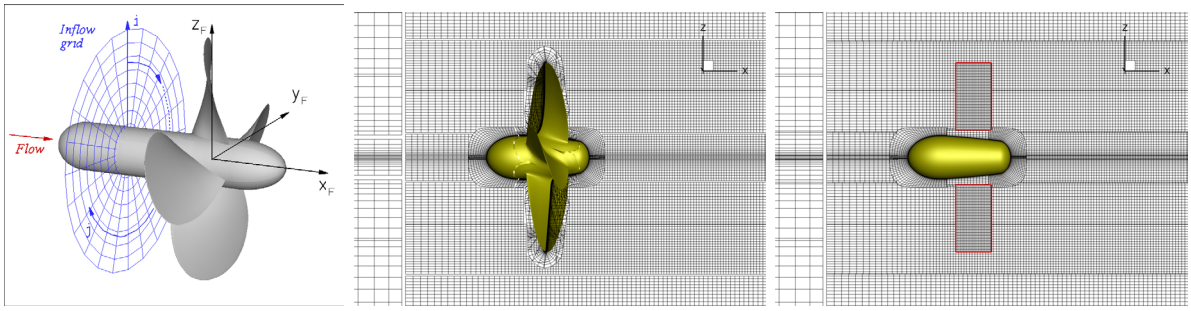

Figure 1: Left: cylindrical coordinate system (x, θ, r) associated to a cartesian frame of reference $(Ox_F y_F z_F)$ fixed with respect to a rotating propeller. Right: computational grids for full RANSE and hybrid RANSE/BEM solvers compared.

The coupling between solutions from RANSE and BEM solvers is achieved through an iterative procedure. As initial step, the inflow to the propeller is estimated from a RANSE solution of the flow field with propeller effects in Eq. (5) set to zero. The resulting initial guess of the inflow is used to perform a propeller flow analysis by BEM and to evaluate propeller loading and body force distributions as described above. Next, body force terms are plugged into the right hand side of Eq. (5) and a new RANSE solution is evaluated. In particular, a new guess of the total velocity field $\mathbf{v}$ is estimated. This velocity distribution is *total* in that propeller effects are included via source terms $\mathbf{Q}$ in the RANSE. Next, a new guess of propeller effects is determined by solving BEM and using the total velocity field $\mathbf{v}$ from RANSE to determine the inflow to the propeller

and impose boundary conditions. Recalling Eq. (3), the impermeability condition on the propeller surface implies that quantity $\mathbf{v}_R = \mathbf{v} - \nabla\varphi$ is evaluated. Quantity $\mathbf{v}_R$ is usually referred to as the *effective inflow*. The evaluation of this quantity implies that the propeller-induced velocity $\nabla\varphi$ calculated by BEM is known at each iteration from the previous step. Thus, a new BEM solution can be evaluated, a new guess of volume force terms is determined and the procedure is iterated until convergence.

In principle, the effective inflow should be evaluated on the actual propeller surface. A reasonable approximation to reduce the computational effort of the BEM solution is to evaluate $\nabla\varphi$ and hence $\mathbf{v}_R$ only over a plane perpendicular to the propeller axis. In the present formulation, this *inflow plane* is located at the inlet section of the RANSE grid block where volume force terms are defined.

Finally, if quantities $\mathbf{g}_k$ in Eq. (8) are averaged over a propeller revolution, a time-averaged distribution of body force terms $\hat{\mathbf{g}}_{l,m,n}$ follows and propeller effects representation like in the actuator disk model is recovered.

3 NUMERICAL RESULTS

The capability of the proposed hybrid RANSE/BEM methodology to describe the hydrodynamic interaction between a rotating propeller and the surrounding viscous flow is investigated by considering the case of an isolated propeller in a uniform onset flow (open water conditions). In spite of its simplicity, this layout is very useful to analyse in details how propeller induced perturbations by BEM are transferred into the RANSE solution in the coupled approach. In particular, vortical and turbulent structures in the propeller wake are clearly identified. Similarly, recalling in open water conditions the only source of perturbations to the flow field is the propeller, the effective inflow to the propeller, $\mathbf{v}_R = \mathbf{v} - \nabla\varphi$ (Sec. 2.3) is theoretically zero and hence it is possible to quantify discrepancies between numerical predictions by the hybrid RANSE/BEM model and the expected flow pattern. Although open water conditions can be simulated by steady–flow simulations by solving either RANSE or BEM equations in a blade-fitted frame of reference, calculations addressed here are performed in fully unsteady mode to investigate the performance of the general RANSE/BEM coupling for transient flows.

The INSEAN E779A four–bladed propeller is chosen as a test case. Main geometry parameters and 3D views of the propeller are illustrated in Fig. 2. Propeller flow simulations are performed at inflow speed V =5 m/s, propeller rotational rate $n = 25$ rps. Recalling $D = 0.227$ m, this yields $J = 0.88$, and $Re = nD^2/\nu = 1.12 \times 10^6$.

The E779A model propeller has been the subject of extensive full RANSE studies by code χ–*Navis* as described in [18]. Numerical results from this reference are used here as benchmark data to assess flow predictions by the hybrid RANSE/BEM model. Unsteady full RANSE computations are performed on four grid levels, the coarser one being obtained by taking every other point of the finer one. The first (finest) grid has a total of 11.3M cells. About 2.4M grid cells are devoted to discretizing the fluid domain surrounding blades.

INSEAN E779A model	
Number of blades	4
Diameter	0.227 m
Expanded area ratio	0.468
Pitch ratio (0.7 R)	1.183
Hub ratio	0.295

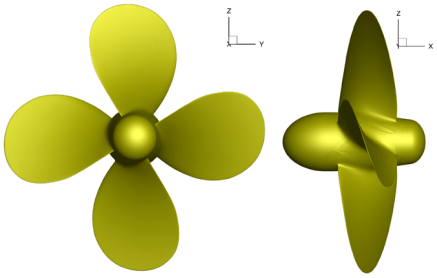

Figure 2: The INSEAN E779A model propeller. Main parameters and 3D views.

Using the hybrid RANSE/BEM model, the CFD grid is the same of the full-RANSE case in [18] except for blade-fitted grid blocks that are unnecessary and replaced by a cylindrical grid block with a basic polar distribution of nodes. As a result, the hybrid approach yields on the finest grid a saving of 2.2M cells with respect to full RANSE case.

Recalling the inflow to the propeller is uniform, calculated flow quantities are expected to be constant in a frame of reference fixed with rotating blades. Local flow quantities are presented as instant distributions at a time step corresponding to an arbitrary position of blades, whereas global quantities (*i.e.*, propeller loads) are averaged over a revolution.

A key of hybrid RANSE/BEM coupling is the conversion of blade surface loads determined by BEM into a surface distribution on blade mean surface of the algebraic sum of suction/pressure side loads (quantity $\mathbf{q}_k$ in Eq. 8). The latter quantity is the basis for the evaluation of volume forces. All related quantities, surface load, mean load and volume force evaluated during the hybrid RANSE/BEM iteration at an arbitrary time step are depicted in Fig. 3. In particular, axial components of mean load and of volume forces are depicted. It is worth noting the regular distribution of volume forces reflecting the actual position of blades during revolution about the shaft axis (blade in the twelve o'clock position chosen here).

Surface loads on blades are integrated to determine propeller thrust and torque using Eq. 4, and results from both full BEM, full RANSE and hybrid RANSE/BEM are compared in Table 1.

Table 1: Comparison of predicted propeller thrust and torque coefficients.

	full BEM	full RANSE	hybrid RANSE/BEM
K_T	0.1582	0.1342	0.1476
$10{\cdot}K_Q$	0.3178	0.2857	0.2990

The next step is to analyse propeller-induced flow by the alternative methodologies. Flow velocity distributions are presented in non dimensional form by using $V_{ref} = \pi nD$ as reference velocity. This yields that nondimensional uniform inflow velocity is 0.28.

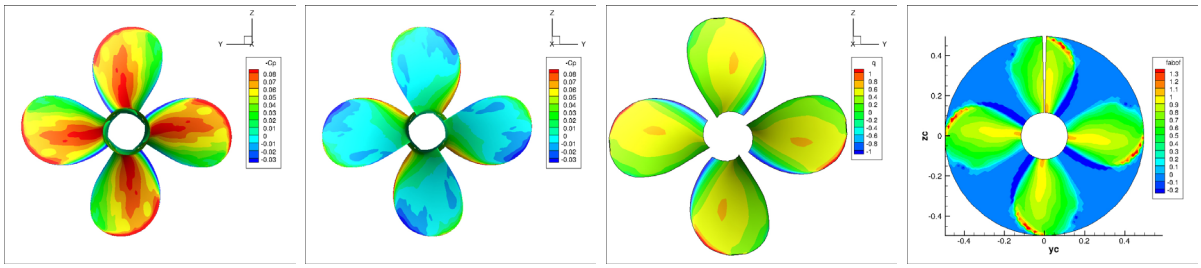

Figure 3: Blade loading representations from BEM solution: from left to right, surface normal load distribution (suction and pressure sides), axial mean load on blades mean surfaces, axial volume forces.

Figure 4 shows distributions of velocity components on a longitudinal plane ($y_{_F} = 0$). Numerical results by the hybrid model and by full RANSE are compared and contourmaps of Cartesian components $u = \mathbf{v} \cdot \mathbf{e}_x, v = \mathbf{v} \cdot \mathbf{e}_y, w = \mathbf{v} \cdot \mathbf{e}_z$ are presented. A general correspondance between wake flow structures in hybrid RANSE/BEM (top) and full-RANSE (bottom) solutions is observed. A closer insight shows that the hybrid model tends to smooth out velocity gradients downstream the propeller region faster than full-RANSE simulations. This is due to the fact the interaction between the fluid and solid boundaries is indirectly represented by equivalent volume forces distributed over a volume resembling the actual position of solid blades. In top Fig. 4 a black box denotes the extension of the volume force grid block.

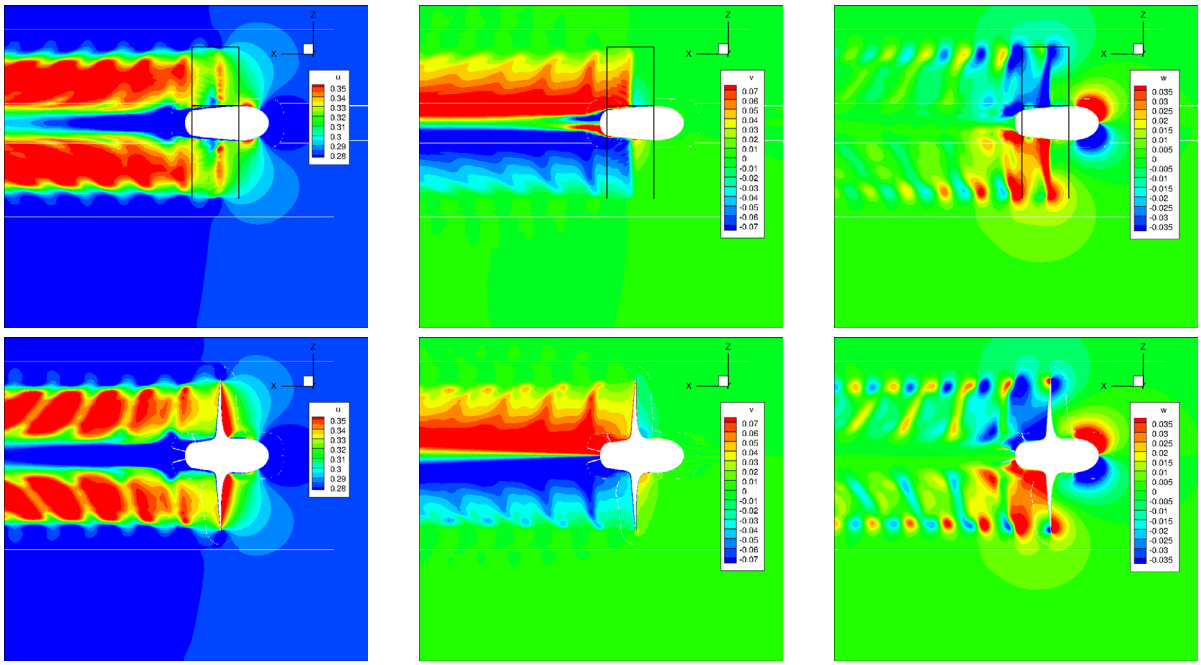

Figure 4: Velocity comp. u, v, w. Plane $y_{_F} = 0$. Hybrid RANSE/BEM (top), full RANSE (bottom).

Figure 5 shows distributions of velocity components on a transversal plane in the propeller wake at $x_F/R = 0.31$. This plane corresponds to the axial position of the outlet section of the volume force grid block. Numerical results by the hybrid model (top) and by full RANSE (bottom) are compared. In this case, axial velocity component u and tangential and radial in-plane components are plotted. Akin previous plots, a qualitative good agreement between hybrid RANSE/BEM and full RANSE results is noted, although regions with highest velocity gradients are slightly smeared out in the hybrid solution.

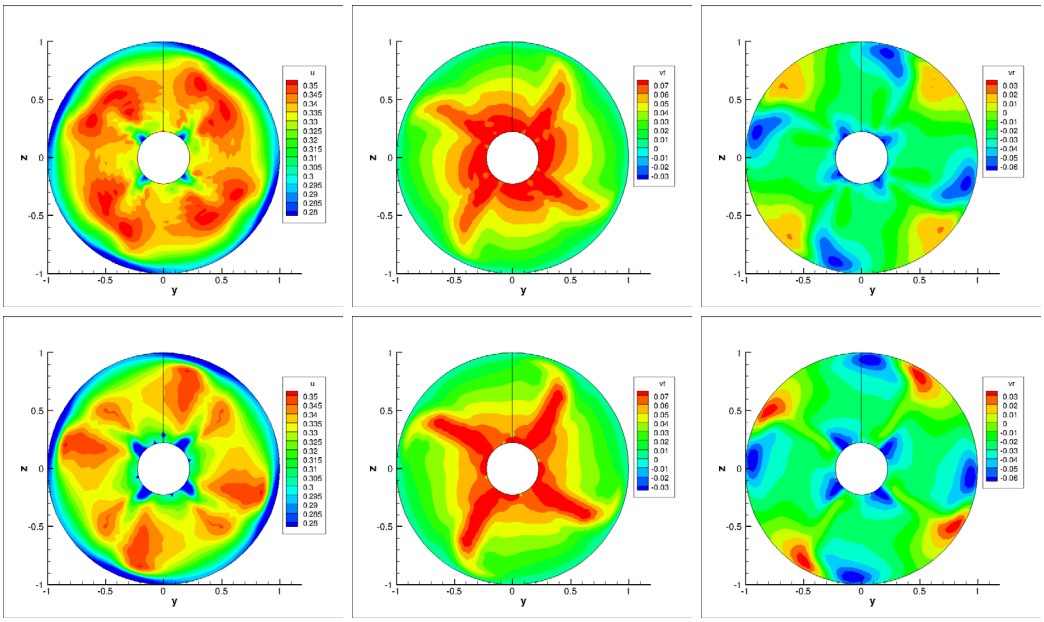

Figure 5: Velocity components u, v_t, v_r at plane $x_F/R = 0.31$. Hybrid RANSE/BEM (top) and full RANSE (bottom).

A quantitative indication of the agreement between hybrid RANSE/BEM and full RANSE results from Fig. 5 is obtained by considering Fig. 6 where velocity components distributions at constant radius on plane at $x_F/R = 0.31$ (top) and $x_F/R = 1.0$ (bottom) are depicted. In particular, radial sections at $r/R = 0.36, 0.71, 0.90, 0.98$ are plotted. A good agreement between hybrid RANSE/BEM and full RANSE results is noted except for the core of the trailing wake, where the hybrid model is not able to reproduce velocity peaks that are detected by a full RANSE solution. A shift along tangential direction θ of results by the tow models is due to the fact that in the hybrid model the blade is represented by a volume force distribution whose thickness is typically larger than the actual thickness of the real blade resolved by full RANSE. This misalignment can be compensated by a few degrees angular shift of hybrid model results.

Next, the velocity field upstream the propeller is analysed. Figure 7 presents distributions of velocity components at inlet plane of the volume force grid block, $x_F/R = -0.31$. Velocity components by hybrid RANSE/BEM present lower values than full RANSE so-

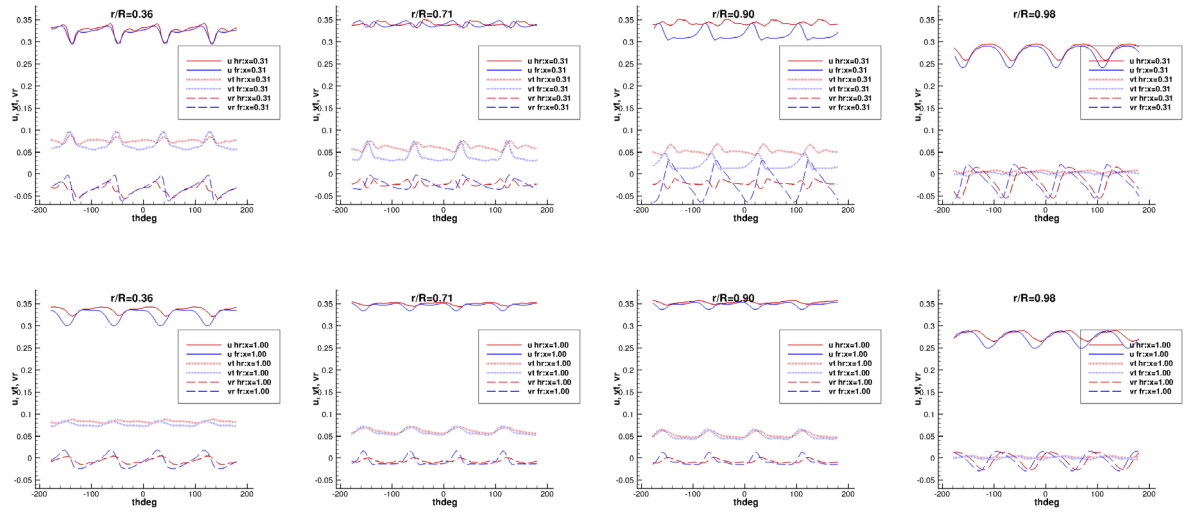

Figure 6: Velocity components u, v_t, v_r at constant radius over planes at $x_F/R = 0.31$ (top) and $x_F/R = 1.0$ (bottom). From left to right: radial sections at $r/R = 0.36, 0.71, 0.90, 0.98$. Hybrid RANSE/BEM and full RANSE results compared.

lution. The hybrid model slightly underestimates the suction effect of the propeller at the inlet section. Differencies at lower radii are partly explained with non-rotating hub in the hybrid model whereas this boundary rotates in the RANSE. Globally, differences are limited to few percent of inflow velocity intensity, with lower averaged axial inflow velocity in the hybrid solution than in the full RANSE. The effect is to determine a virtually lower advance ratio J for hybrid model simulations. It is worth observing that such lower inflow speed is consistent with slightly higher propeller loads predicted by the hybrid model than by full RANSE, as given in Table 1 above. Recalling Section 2.3, the effective inflow is a fundamental quantity for the exchange of information between viscous and inviscid flow solver in a hybrid RANSE/BEM approach. Left Fig. 8 shows the axial component of the effective inflow. Velocity is non-dimensional with respect to unperturbed onset flow speed. It may be noted that except for a region close to the hub and blade leading edge, the effective inflow is close to zero as expected in open water conditions. Results in left Fig. 8 refer to time–accurate simulations, whereas results on the right correspond to the hybrid RANSE/BEM solution in steady-flow conditions under the implicit assumption that the inflow to the propeller is axisymmetric. Comparing the two results it is apparent that time averaging determines lower effective inflow values.

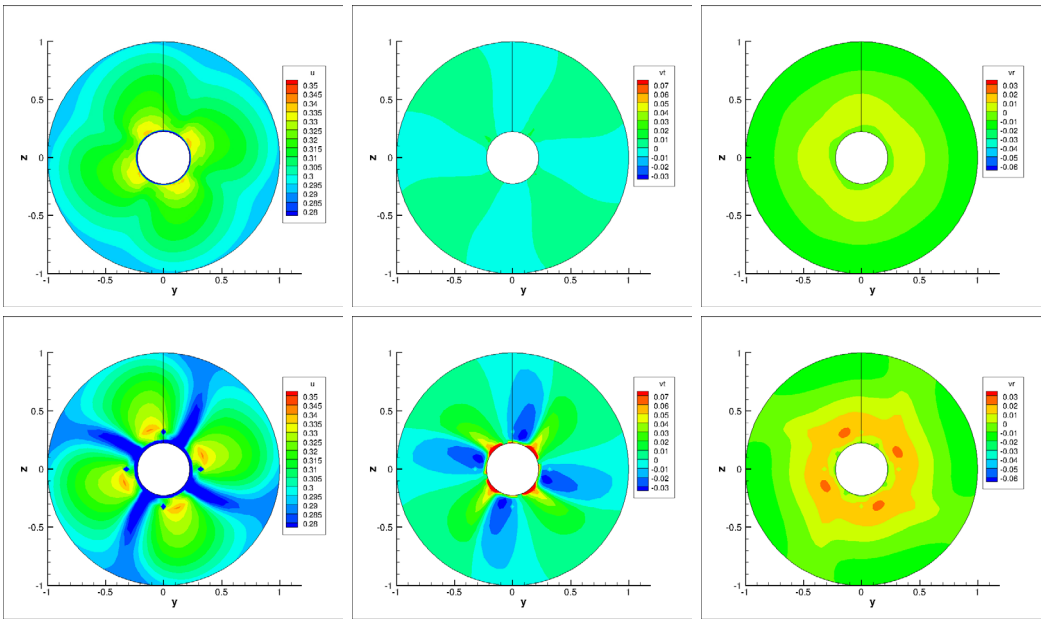

Figure 7: Velocity components u, v_t, v_r at plane $x_F/R = -0.31$. Hybrid RANSE/BEM (top) and full RANSE (bottom).

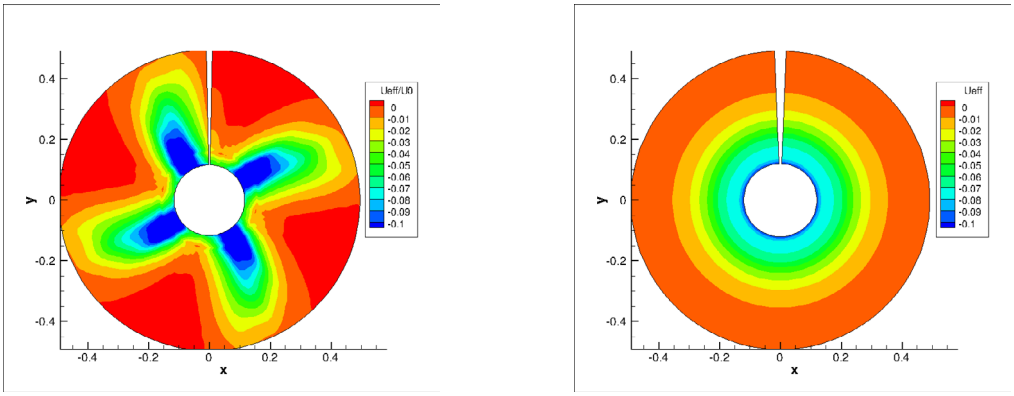

Figure 8: Effective inflow distribution (axial component) under time–accurate hybrid RANSE/BEM (left) and by steady flow assumptions (right).

4 CONCLUSIONS

The development of a hybrid viscous/inviscid model for the computational analysis of propulsor–ship interactions under arbitrary unsteady–flow conditions have been described. The proposed methodology generalises standard actuator disk models in that the coupling between viscous and inviscid flow solvers is enforced in a time-accurate fashion. The computational methodology is based on the coupling of unsteady RANSE and BEM models in-house developed at CNR-INSEAN.

Numerical applications have been presented to investigate the capability of the pro-

posed hybrid RANSE/BEM model to describe transient flow features that characterize the interaction between a rotating propeller and the surrounding flow, *e.g.*, a hull wake in case of a fully appended ship.

Numerical results from the hybrid RANSE/BEM model have been compared with full RANSE solutions for a case study describing a propeller in open water. Results of this comparative study highlight a general good agreement of predicted flow fields by the two approaches. In particular, propeller loads and trailing wake flow structures are correctly described by the hybrid model. Recalling the strong reduction of computational burden of the hybrid model as compared to full RANSE simulations, the proposed methodology can be considered as a computationally efficient alternative to full RANSE for applications to ship design and optimization problems.

Extensive computational studies are in progress to investigate model features that may have an impact on the quality of flow predictions and to apply the methodology to the analysis of ship propulsion simulations.

REFERENCES

[1] Sparenberg, A. On the potential theory of the interaction of an actuator disc and a body. *Journal of Ship Research* (1972) **16**:271-277.

[2] Schetz, A., Favin, S. Numerical solution for the near wake of a body with propeller. *Journal of Hydronautics* (1977) **11**:136-141

[3] Zhang, D.H. Numerical Computation of Ship Stern/Propeller Flow. *Doctoral Thesis*, Chalmers University of Technology, Gothenburg, Sweden, 1990.

[4] Rijpkema, D., Starke, B., Bosschers, J. Numerical simulation of propeller-hull interaction and determination of the effective wake field using a hybrid RANS-BEM approach. Third International Symposium on Marine Propulsors (SMP), Launceston, Tasmania May 2013.

[5] Deng, G. B, Queutey, P., Visonneau, M., and Salvatore, F. Ship propulsion prediction with a coupled RANSE-BEM approach. *Fifth Int. Conference on Computational Methods in Marine Engineering, MARINE 2013,* Hamburg, Germany, May 2013.

[6] Greve, M., W ockner-Kluwe, K., Abdel-Maksoud, M., Rung, T. Viscous-Inviscid Coupling Methods for Advanced Marine Propeller Applications. *International Journal of Rotating Machinery* (2012).

[7] Morino, L., Salvatore, F., Gennaretti, M. A New Velocity Decomposition for Viscous Flows: Lighthill's Equivalent–Source Method Revisited. *Computer Methods in Applied Mechanics and Engineering*, (1999) **173**(3–4):317–336.

[8] Greco, L., Salvatore, F., Di Felice, F. Validation of a Quasi–potential Flow Model for the Analysis of Marine Propellers Wake. *Twenty-fifth ONR Symposium on Naval Hydrodynamics*, St. John's, Newfoundland, Canada, August 2004.

[9] Pereira, F., Salvatore, F., Di Felice, F. Measurement and Modelling of Propeller Cavitation in Uniform Inflow. *Journal of Fluids Engineering* (2004) **126**:671–679.

[10] Calcagni, D., Greco, L., Salvatore, F. Numerical Assessment of a BEM-based Approach for the Analysis of Ducted Propulsors. *NuTTS 2009 Conference,* Cortona, Italy, October 2009.

[11] Salvatore, F., Greco, L., Calcagni, D. Computational analysis of marine propeller performance and cavitation by using an inviscid-flow BEM model. *Second Int. Symposium on Marine Propulsion, SMP 2011*, Hamburg, Germany, June 2011.

[12] Calcagni, D., Salvatore, F., Muscari, R., Sundberg, J., Johansson, R. Computational Analysis of Contra-Rotating Podded Propulsors Using a Hybrid RANSE/BEM Model. *Eleventh International Conference on Hydrodynamics, (ICHD 2014)*. Singapore, October 2014.

[13] Morino, L. Boundary Integral Equations in Aerodynamics. *Applied Mechanics Reviews* (1993) **46**(8):445–466.

[14] Di Mascio, A., Broglia, R., Muscari, R., and Dattola, R. Unsteady RANS Simulation of a Manoeuvring Ship Hull. *25th Symposium on Naval Hydrodynamics*, St. John's, Newfoundland, Canada, August 2004.

[15] Muscari, R. and Di Mascio, A. Simulation of the flow around complex hull geometries by an overlapping grid approach. *Proc. 5th Osaka Colloquium on advanced research on ship viscous flow and hull form design by EFD and CFD approaches*, Osaka, Japan, 2005.

[16] Muscari, R., Broglia, R., and Di Mascio, A. An overlapping grids approach for moving bodies problems. *Proceedings of the 16th International Offshore and Polar Engineering Conference (ISOPE 2006)*, San Francisco, California, USA, 2006

[17] Muscari, R., Felli, M., and Di Mascio, A. Analysis of the Flow Past a Fully Appended Hull with Propellers by Computational and Experimental Fluid Dynamics. *ASME J. Fluids Eng.* (2011) **133**(6).

[18] Muscari, R., Di Mascio, A., Verzicco, R. Modeling of vortex dynamics in the wake of a marine propeller *Computers & Fluids* (2013) **73**:6579.